The Cryosphere Discuss., 4, 1–30, 2010
www.the-cryosphere-discuss.net/4/1/2010/


The Cryosphere Discussions

This discussion paper is/has been under review for the journal The Cryosphere (TC).
Please refer to the corresponding final paper in TC if available.

# Spatial and temporal variability of snow depth and SWE in a small mountain catchment

**T. Grünewald, M. Schirmer, R. Mott, and M. Lehning**

WSL Institute for Snow and Avalanche Research SLF, 7260 Davos Dorf, Switzerland

Received: 22 December 2009 – Accepted: 23 December 2009 – Published: 13 January 2010

Correspondence to: T. Grünewald (gruenewald@slf.ch)

Published by Copernicus Publications on behalf of the European Geosciences Union.





## Abstract

The spatio-temporal variability of the mountain snow cover determines the avalanche danger, snow water storage, permafrost distribution and the local distribution of fauna and flora. Using a new type of terrestrial laser scanner (TLS), which is particularly suited for measurements of snow covered surfaces, snow depth, snow water equivalent (SWE) and melt rates have been monitored in a high alpine catchment during an ablation period. This allowed for the first time to get a high resolution (2.5 m cell size) picture of spatial variability and its temporal development. A very high variability in which maximum snow depths between 0–9 m at the end of the accumulation season was found. This variability decreased during the ablation phase, although the dominant snow deposition features remained intact. The spatial patterns of calculated SWE were found to be similar to snow depth. Average daily melt rate was between 15 mm/d at the beginning of the ablation period and 30 mm/d at the end. The spatial variation of melt rates increased during the ablation rate and could not be explained in a simple manner by geographical or meteorological parameters, which suggests significant lateral energy fluxes contributing to observed melt. It could be qualitatively shown that the effect of the lateral energy transport must increase as the fraction of snow free surfaces increases during the ablation period.

## 1 Introduction

The largest part of annual winter-precipitation in the Alps above 1000 m a.s.l. falls as snow and most of it is stored for the season in the snow cover. When snow melt starts at the end of the accumulation season, the water is returned to the hydrologic cycle. Amount and timing of the melt strongly depend on thickness and spatial distribution of the snow cover. Hence the spatial and temporal variability of the snow cover has a high impact on the alpine water balance and strongly affects nature and mankind (Elder et al., 1998). For instance, the supply with drinking water and energy, agriculture and





vegetation growth, all strongly depend on snow cover and alpine water storage (e.g. Armstrong and Brown, 2008; Jones et al., 2001; Keller et al., 2000). On the other hand, rapid melting can cause flooding and increased erosion (e.g. Pomeroy and Gray, 1995; Male and Gray, 1981). Furthermore, winter tourism with its high economic importance in many alpine regions, strongly depends on snow reliability and snow cover duration (e.g. Beniston, 2000; Haefner et al., 1997; López-Moreno and Nogués-Bravo, 2006; Fazzini et al., 2004; Marty, 2008).

To make reliable assessments of current and future snow dynamics, it is essential to obtain a better understanding of the total amount of snow stored in a catchment and how snow cover changes in space and time, especially in the ablation period.

A lot of work has been carried out on the spatial variability of snow depth and snow water equivalent (SWE) and how it is influenced by meteorological and topographical factors on different scales (e.g. Blöschl, 1999; Merz et al., 2009; Liston and Sturm, 2002; Balk and Elder, 2000; Pomeroy et al., 2003; Deems et al., 2006; Trujillo et al., 2007; Mott et al., 2008; Dadic et al., 2010). In particular, snow deposition and snow transport due to wind have been investigated in much detail (e.g. Doorschot et al., 2001; Lehning et al., 2008) and it has been shown that snow distribution influences runoff dynamics in mountain catchments (Lehning et al., 2006). Many of these efforts, however, are based on model studies and suffer from insufficient validation against measurements. Very often, limited snow depth and SWE observations are extrapolated to large areas using statistical models (e.g. López-Moreno and Nogués-Bravo, 2006; Marchand and Killingtveit, 2004; Chang and Li, 2000; Luce et al., 1999; Erickson et al., 2005).

A promising attempt to gain area-wide high resolution snow depth data is the introduction of lidar altimetry to snow sciences. Airborne laser scanning (ALS) was proofed to be an appropriate and accurate method for gathering area-wide snow depth measurements (Deems and Painter, 2006; Hopkinson et al., 2001). ALS data was used to investigate spatial variability and scale invariance of snow depth and its relationship to wind direction, vegetation and topography for several mountainous test sites (Deems




et al., 2006; Trujillo et al., 2007).

In recent years, the introduction of terrestrial laser scanning (TLS) to snow science has given a further push forwards as this technology provides the possibility to do more cost effective and flexible area-wide snow depth observations with high spatial resolution (Bauer and Paar, 2004; Jörg et al., 2006; Prokop, 2008). Prokop et al. (2008) and Schaffhauser et al. (2008) performed detailed investigations on the accuracy of TLS for measuring snow depth. Both studies arrive at the conclusion that TLS is an appropriate tool for mapping snow depth with high accuracy.

However, no studies exist which use this promising technique to focus on snow depth and SWE distribution and their time development for a catchment. By performing repeated TLS measurement campaigns in the Albertibach-catchment (Davos, Switzerland) for the whole ablation season of winter 2007/08, we present a unique data set of snow depth and SWE variability in a high mountain setting: the repeated catchment-wide measurement campaigns offer the possibility to investigate seasonal snow cover changes by looking at snow depth changes (mostly depletion) during the ablation phase.

This paper presents a first qualitative and quantitative investigation of this unique dataset. We first give an overview on the study site and the methods used for collecting, processing and analysing the data in the method and data section. Then a section on results and discussion of the data and findings is given before ending the paper with a conclusion of the main results of the study and a short outlook on future tasks and challenges.

## 2 Method and data

### 2.1 Site description

The area of investigation is a small high mountain catchment located in the region of Davos (Switzerland) (Fig. 1). The area of interest is defined by the drainage area of





the Albertibach, which discharges in an easterly direction and is surrounded by steep mountain ridges to the North and South. The elevation of the area ranges from 1940 to 2658 m a.s.l. and is located above the local tree line. The total size of the catchment area is 1.3 $km^2$, of which we covered 0.6 $km^2$ (46%) in the laser surveys. The scanned area can be regarded as representative for the whole catchment in terms of elevation range, aspect, and slope.

The site is well equipped with a dense network of seven meteorological stations, which provide a continuous series of meteorological data.

### 2.2 Measurement methodology and accuracy assessment

We carried out four measuring campaigns to collect the data used in this study in winter 2007/08. The first survey was made at the end of the accumulation season (26 April 2008) and we continued at intervals of about two weeks until the end of the melting season (13 May, 2 June and 10 June 2008).

To investigate area wide snow depth, we used a *Riegl LPM 321* terrestrial laser scanner (Riegl, 2008). With a wavelength of 905 nm, the *LPM 321* operates in a wavelength where the reflectivity of snow is very high. As the maximal distances we measured were below 1000 m, it was possible to scan in the *LPM*'s near range mode (up to 1500 m), which provides the best spatial resolution and accuracy. Detailed information how to measure snow depth with TLS can be found in Prokop (2008).

We subjected all laser data to a variety of quality checks, in particular, we compared the laser measurements with measurements obtained from a tachymeter, as described in Prokop et al. (2008). The quality control revealed that snow depths showed mean deviations in z-direction of less than 4 cm and standard deviations of less then 5 cm at distances of up to 250 m. This is a higher level of accuracy than that published by Prokop et al. (2008) and more than sufficient for our purposes. Furthermore, an airborne laser scan (ALS) is available for the end of the accumulation season using an independent helicopter based technology (Skaloud et al., 2006; Vallet et al., 2005). With this data, it was possible to investigate whether there are systematic errors in the

terrestrial scans. The analysis showed that the ALS had a mean deviation of less than 5 cm against the tachymeter survey, which took place at the same time. The standard deviation was 6 cm. The spatial distribution of the deviation in z-direction between the ALS and the TLS survey for 26 April is shown in Fig. 2. Comparing TLS and ALS gave a mean deviation of 10 cm and a standard deviation of 13 cm. The difference between TLS and ALS increased with the distance measured by the TLS as is clearly visible in Fig. 2 (blue colours). This might be due to the TLS being less accurate over long distances but the accuracy is still more than sufficient for the analysis presented here.

### 2.3 Data processing

TLS does not measure snow depth directly but the point distances from the scanner to the surface of the targets (snow surface) with high spatial resolution and accuracy. To get absolute snow depths, the scans must be subtracted from a digital elevation model (DEM). The DEM used in this study was created from a summer TLS survey using the same technology.

We produced raster maps of snow depth data with a cell size of 2.5 m for each survey. Furthermore, we calculated the average daily snow depth change between two succeeding surveys for every raster cell. To avoid erroneous daily snow depth changes for pixels which showed a complete melt out before the later survey, we removed those cells from the analysis. This was done by creating a binary raster mask from the colour information in the orthophotos, which were also taken during the TLS surveys. These masks were then applied to maps of snow depth and snow depth change which are analyzed below.

To calculate SWE from snow depth data, average snow cover density estimations are necessary. Many studies have found that the spatial variability of SWE is relatively small in comparison to snow depth (e.g. Pomeroy and Gray, 1995; Marchand and Killingtveit, 2004; Dickinson and Whiteley, 1971). Consequently, it is common to estimate areal SWE with a small number of representative density measurements and a high number of snow depth data (e.g. Rovansek et al., 1993; Elder et al., 1998; Jonas

et al., 2009). Thus, we calculated SWE based on a small number of well selected density measurements. Depth-average snow density is often assumed to be controlled by a small number of topographical and meteorological parameters which are total snow depth, elevation, solar radiation, climatic region and vegetation patterns (e.g. Jonas et al., 2009; Anderton et al., 2004). Because of the limited extent of the investigation area, we only focus on snow depth and solar radiation in this study.

To ascertain wether there was a significant dependency between the snow density ($\rho$) and solar radiation, we classified the investigation area into three sub-areas using total potential incoming solar radiation for the particular time periods between two investigations, as simulated with the physical based model *Alpine3D* (Lehning et al., 2006; Helbig et al., 2009). For each radiation class, we took three manual SWE-measurements at locations with different snow depths (HS) (<50 m, 50–100 cm, >120 cm). Thus we obtained a depth dependent average density, $\rho(R,t)$, for each radiation class ($R$) and each time step ($t$). To test the significance of the dependencies $\rho(R)$ and $\rho t$ we used the Kruskal-Wallis test. The tests showed that there were significant differences for the specific time steps $\rho(t)$ but no significant dependency on radiation class $\rho(R)$ could be found. We also investigated if a direct relationship between HS and $\rho(t)$ was obvious from the measurements but no general trend could be found. We hence decided to use a single $\rho(t)$ for each time step which translates snow depth to SWE:

$$\mathrm{SWE} = \rho(t)\mathrm{HS} \quad (1)$$

where SWE is in mm and HS in m. A summary of the calculated $\rho(t)$ values are given in Table 1.

As a next step, we produced maps with the total SWE using Eq. (1) and average daily "melt rate", which is simply taking the SWE rate of change between consecutive laser scans. The so called melt rate can include contributions from snow falls, settling, snow transport, snow sublimation and true melting. As the SWE maps are the results of a simple linear relationship as given in Eq. (1), the patterns of the snow depth maps

and the SWE maps are identical for each single time step. Hence we will focus our analysis on SWE-maps only and give the values for snow depth in brackets where appropriate. Since $\rho$ is time dependent, the melt rate and snow depth change maps did not show exactly the same patterns. But as there were no relevant differences in the characteristic features we only show the results obtained from the daily melt rates in what follows.

To refine the analysis, we separated two sub-areas from the investigation area (Fig. 1) based on the visual impression that two different snow distribution patterns may dominate these two sub-areas: the first covers the north-easterly exposed slopes of Wannengrat, and will be referred to as NE in the following. It is characterized by a highly variable snow deposition on a rather large scale. The second sub-area consists of the south-facing slopes of the Vordere Latschüel (VL), which appears to have a rather homogeneous snow distribution.

### 2.4 Data analysis

A quantitative analysis of the raster maps allowed a detailed evaluation of the spatial and temporal variability of SWE, on the one hand, and the average melt rates, on the other hand. We first visually interpreted the maps to identify obvious surface structures and characteristics. To quantify the spatial variability and changes in time, histogram plots for the distribution of SWE and the average melt rates between the individual scans were examined. Furthermore, we investigated basic statistics such as mean ($\mu$), standard deviation ($\sigma$) and total snow volume for each time period. As described above, the statistical parameters always refer to the snow-covered area. We then focused on possible statistical dependencies of the melt rate in the investigation area on topographic and meteorological parameters. For this purpose, the Pearson's linear correlation coefficient for the melt rate as dependent variable.was calculated. As independent variables we used:

– Topographical parameters derived from the DEM: altitude, slope, northing (differ-

ence in degrees from north).

- Mean daily sum of incoming solar radiation, simulated with the physical based model *Alpine3D* (Lehning et al., 2006; Helbig et al., 2009), for each period of two succeeding surveys. As input data for the model, we used data derived from an automatic weather and snow station located in the catchment. The model then produced hourly output for incoming shortwave radiation for each grid-cell of a 10 m-raster. We then averaged the output to one mean radiation day for each of the three periods.
- SWE at the end of the accumulation season ($SWE_{max}$) derived from TLS survey.
- Local windspeed obtained from high resolution flow fields; simulated with the mesoscale atmospheric model ARPS (Xue et al., 2000; Mott et al., 2008; Raderschall et al., 2008; Mott and Lehning, 2010). The three-dimensional windspeed was modelled on a horizontal grid resolution of 5 m. The local flow fields were calculated for a north-westerly and a south-westerly wind situation, which were observed to be the predominant wind directions for the three periods between the scans. Note that for the first period both wind situations occurred but the north-westerly situation dominated. In contrast, in the second period, both prevailing wind direction occurred with a similar frequency. A major foehn event occurred in beginning of this period. In the third period only north-westerly wind situations were observed.

To account for possible interactions between these parameters, we combined the variables mentioned above, in multiple linear regression models. Only the models which performed best will be shown in the following.

## 3 Results and discussion

### 3.1 Time development of SWE distribution

A map of the spatial SWE distribution in the investigation area for the end of the accumulation season (26 April) is shown in Fig. 3a. At that point of time, the whole catchment was snow covered, with exception of small snow-free patches in the steep rock faces in the south and north-west of the area. SWE averaged to 696 mm (HS 2.0 m) and peak SWE was 3120 mm (HS 9.0 m). Those exceptional large snow depths were mainly located at two cornice-like drifts which had formed at the steep north-easterly exposed slopes of the Wannengrat summit due to drifting and blowing snow. Areas with above average SWE could also be found in the steep south facing slopes of the Vordere Latschüel (VL). The flatter areas of the Chilcher Berg clearly showed average or below average SWE. But line-like features with above average SWE were also clearly visible in that area. From the DEM and a topographic map we could identify those features as ditches which were packed with snow probably due to snow transport processes (Lehning et al., 2008).

The following scan, 17 days later, showed predominantly unchanged spatial patterns (Fig. 3b): the cross-slope accumulation zones in the NE remained the dominant feature till the end of the ablation season while snow depth in the VL suffered stronger decrease than average (Fig. 3c, d; see also Fig. 6). A significant number of snow-free patches emerged especially on the knolls and ridges where SWE was lowest in the beginning of the ablation season. Complete melt out propagated quickly from those first snow-free areas in the course of time. This may be because of lower snow depths at the edges of the snow patches or because of lateral advective transport of heat from the warmer snow-free surfaces onto the colder snow cover (Essery and Pomeroy, 2004), which will be discussed in detail below.

Histogram representations of the distributions of SWE at the time of each scan are shown in Fig. 4. Mean snow depth was decreasing continuously (26 April=2.0 m, 13 May=1.5 m , 2 June=1.3 m, 10 June=1.1 m) but mean SWE values remained on

a similar level for all time steps (26 April=697 mm, 13 May=569 mm , 2 June=570 mm, 10 June=559 mm), which is interesting and counter-intuitive at first. This finding is, to a smaller degree, explained by the increasing snow densities (Table 1), which partly balanced the effect of decreasing mean snow depth for the last three surveys. The increase in snow density can be explained by processes like settling, moisture penetration or melt – refreeze processes of the snow cover. More importantly, however, the snow covered area, to which the statistics are referring to, changed in time – the later in the season, the smaller was the snow-covered area due to melt out of significant portions of the catchment. Areas which only had a shallow snow cover at peak accumulation were lowering the mean SWE at that time in comparison to the later surveys when those areas were bare and did no longer contribute to the statistics. An analysis of the statistics, which only include those raster cells which were still snow covered in the last survey, confirmed this hypothesis: the mean SWE values were now much higher at the peak of snow accumulation (Fig. 4b) and decreased with time (26 April=1248 mm, 13 May=1025 mm , 2 June=769 mm, 10 June=581 mm).

This effect of snow density and snow covered area at the time of each scan was also visible in the standard deviation values ($\sigma$), which were used to quantify the spatial variability of the data: $\sigma$ of snow depth, referring to the snow covered area, was 1.3 m at the end of the accumulation season and decreased continuously (13 May=1.1, 2 June=1.0) to 0.9 m at the end of the ablation season whereas $\sigma$-values for SWE (450–460 mm) remained similar until the last survey. Nevertheless, it can be seen that the spatial variability of both, snow depth and SWE was high for all time steps.

Figure 4b also shows that the histogram graphs for SWE are characterized by similar shape for all time steps and that the only change was a shift towards smaller values. This means that the variability of SWE remained constant while mean SWE decreased when only considering the areas which had not melted out completely at the time of the last survey. Looking again at the histogram graphs which contain the complete area, which was snow-covered at the time of the respective survey, clearly indicates a different behaviour with a changing shape of the SWE distribution (Fig. 4a) as an





effect of the difference in snow-covered area. The decrease in snow-covered area had a major effect on the volume of SWE stored in the catchment, which was $3.3\times10^5$ m$^3$ at 26 April and steadily depleted to $0.7\times10^5$ m$^3$ at 10 June.

Comparing the two sub-areas, VL and NE, clearly shows differences in the distributions of SWE (Fig. 5a, b). The cross-slope accumulation zones (discussed above) which featured the areas maximums SWE were located in NE. Mean SWE with 1059 mm (HS=3.1 m) were therefore larger in the NE than in the VL with 919 mm (2.7 m) at the end of the accumulation season. A higher variability could also be observed in the NE ($\sigma$=569 mm/1.7 m) than in the VL ($\sigma$=335 mm /1.0 m) at the end off the accumulation season. This finding is also obvious from Fig. 3, where the more homogenous snow depth values in the VL are clearly visible. The context of higher variability and higher mean SWE in the NE remained dominant during the whole ablation season.

### 3.2 Spatio-temporal variability of melt rates and their correlation with simple weather and terrain parameters

Melt rates are shown in Fig. 6 and the corresponding histograms are shown in Fig. 7 for all three investigation periods. For the period from 26 April to 13 May the spatial differences between the highest melt rates in the steep south facing slopes and the lowest rates in the northern exposed slopes are clearly visible in Fig. 6a and represent the distribution of potential radiation. The average melt rate was 15 mm/d ($\sigma$=7 mm/d) for this period and rose to 16 mm/d ($\sigma$=7 mm/d) for the second and 30 mm/d ($\sigma$=12 mm/d) for the last period (Fig. 7). This increase can be explained by the larger amount of energy available for melting later in the hydrological season. It has to be noticed that no distinct change occured between the first and the second period due to cool and moist weather during the second period but that both, $\mu$ and $\sigma$ strongly increased in the last period. While the spatial variability of SWE was quite constant, the spatial variability of the melt rates was increasing with time (Fig. 6 and Fig. 7a). The spatial distribution of the melt rates appeared to be more random and may show a smaller direct correla-

tion with topographic factors. This temporal change in variability and spatial patterns might be explained by a shift of the dominating processes which had an impact on the melting: in the first two periods, the energy available for melting was dominated by shortwave radiation which is also indicated by the relatively strong correlation coefficient for shortwave radiation ($r$=0.3) described below. Later in the hydrological season the rapidly increasing fraction of snow free areas leads to changes in the energy balance: the surface albedo of snow free patches is small and causes higher surface temperatures and higher values of lateral sensible heat fluxes and longwave radiation, which then lead to increased melting of the surrounding snow patches (Essery and Pomeroy, 2004) especially at the edges of the patches. Thus, big differences in melting between small and larger snow patches may occur. Nonetheless, a comparison of coefficient of variation values ($CV=\sigma/\mu$) showed that the spatial variability of the melt rates with $CV$ – values of 0.4–0.5 was lower than the spatial variability of snow depth and SWE ($CV$=0.6–0.8), even for the latest time period, where the scatter in melt rates was largest. As can be seen in Fig. 3, as the consequence, the relatively low variability of the melt rates cannot substantially alter the spatial structure of SWE, which was determined during the accumulation season. As an example, both pronounced accumulation zones in sub-area NE remained visible for the whole period of investigation. Thus, the effects of spatially variable melting on snow depletion are smaller than the effect of the snow distribution at the end of the accumulation season. Snow remains there, where most snow was accumulated during the accumulation season. This interpretation is consistent to the findings of Anderton et al. (2004), who stated that spatial patterns of snow disappearance were largely determined by the distribution of SWE at the start of the melt season, rather than by spatial variability in melt rates during the melt season. Their results based on manual surveys are now confirmed by our more detailed dataset.

Similar to the study of Anderton et al. (2004), we could only identify weak correlations between the melt rates on the one hand, and the explanatory topographic and meteorological parameters, on the other hand. Pearson's linear correlation coefficients





are shown in Fig. 8 for all parameters and each time interval: altitude, slope, northing (each $r$=0.4), solar radiation ($r$=0.3) and windspeed$_{SW}$ ($r$=0.3) provided the best correlations for the first period (26 April–13 Mai). For the second period (13 May–2 June) all high correlations from the first period strongly decreased (slope: $r$=0.3, altitude, northing each $r$=0.1, radiation $r$=0, windspeed$_{SW}$=0.2) whereas SWE$_{max}$ gave the best correlation with $r$=−0.4. In the final period (2 June–10 June) all correlations became very weak. This finding again suggests that the factors which dominate melt change in time. The strong decrease of the correlation is in this context attributed to the raising heterogeneity of the surface and of its energy balance which we already described above. The later in the ablation season, the smaller the direct influence of the parameters and the more "random" the melt pattern appears. It is important to note that the melt pattern is not really random but determined by the distribution of snow free patches in the vicinity, which is not represented in local correlations. A further surprising outcome is the decrease of the correlation coefficient for windspeed$_{SW}$, although a major foehn event occurred in the second period. Local high windspeeds promote turbulent fluxes and therefore affect the local energy balance. But advective effects as discussed above would not show up in such a local analysis and require a more involved analysis, which we plan to carry out in future.

The weak correlations become even more clearly when analysing the scatterplots of the melt rates against the predicting parameters. A scatter plot of melt rates against slope angle is shown in Fig. 9. The massive scattering of the data clearly illustrates that high statiscical correlations can not be expected form these data.

These findings lead to the conclusion that none of the simple univariate parameters was adequate to explain spatial melting characteristics in a satisfactory degree. A possible additional factor other than lateral energy transport discussed above may be that the spatial resolution of 2.5 m, may still be too coarse. Windspeed was modelled on a spatial resolution of 5 m. A smaller horizontal resolution would strongly influence the local windspeed distribution (Mott and Lehning, 2010). Patterns which were caused by the micro-relief are not captured by that resolution. Furthermore, there may be





differences between the modelled meteorological variables and the true distribution, e.g. incoming radiation neglects frequent convective clouds over mountain tops.

To examine if interactions between the topographical and meteorological parameters might play a role, we built several multiple linear regression models, for which we tested different factor combinations. For the construction of the regression models, the variables were scaled linearly to [−1;1], to allow a direct comparison of the coefficients. Similar to the univariate correlation analysis, different models performed best for the individual periods: the best fit for the first period is given in Eq. (2) and resulted in an $r^2$ of 0.4. Additional factors and factor combinations could not significantly improve the fit.

$$\text{rate}_1 = 4.2 \cdot \text{altitude} + 7.6 \cdot \text{slope} + 5.6 \cdot \text{northing} + 3.8 \cdot \text{radiation} + 12.2 \quad (2)$$

For the second period an $r^2$ of 0.3 was obtained from the model described in Eq. (3). Most variables which performed best in linear correlation analysis were also showing up in the multiple regression model, but in slightly different order. *Slope* was the most important variable in Eq. (2) and $\text{SWE}_{\text{max}}$ accounted for the highest coefficient in Eq. (3).

$$\text{rate}_2 = -2.1 \cdot \text{altitude} - 8.8 \cdot \text{slope} - 13.6 \cdot \text{SWEmax} + 7.9 \cdot \text{windspeed}_{\text{NW}} + 18.2 \quad (3)$$

The last period did not give remarkable correlations as discussed above. Like already seen in the univariate correlations, we could observe a decrease in correlation with time and this was confirmed by the multiple regressions. Therefore, the influence of topography and meteorology on melt rates gets consistently weaker later in the ablation season. Using f-test, all regressions were found to be highly significant ($p<0.001$) which is not surprising when taking the large size of the sample ($N>18\,000$) into account.





## 4 Conclusions

This contribution presents first results from a rich data set on the spatio-temporal variability of snow depth. It is assumed that a high correlation between SWE and snow depth (HS) allows a simple interpretation of snow depth in terms of SWE (Eq. 1) and therefore most of the analysis is presented for calculated SWE maps and their temporal changes, which are named "melt rate" maps although they are strictly the sum of real melt, sublimation and occasional smaller snowfalls.

Quality checks of the TLS measurement system against independent tachymeter and airborne laser scanning measurements have shown good accuracy of the snow depth measurements such that the analysis presented appears not to be limited by measurement problems.

A striking result from the analysis of SWE development during the ablation phase is that a very variable distribution of "melt rates" is observed. We conclude that qualitatively advective transport of melt energy from snow free areas to remaining snow patches is a major source for this variability and leads to accelerated melt in the course of the ablation period in agreement with earlier results, which have been based on theoretical considerations (Essery and Pomeroy, 2004). This conclusion is consistent with the observation that initial weak correlations of melt rates with obvious meteorological and terrain parameters become even weaker towards the end of the ablation period.

Beyond the first analysis presented here, the data set allows significant further and more in depth work, which we are currently undertaking. A major effort is devoted to a more quantitative understanding of lateral energy transport discussed above by using a combination of a meteorological with a detailed surface process model (*ARPS*/*Alpine3D*: Mott and Lehning, 2010). The most direct application is an assessment of total snow water storage as compared to interpolations made from flat field snow stations (e.g. Bocchiola et al., 2008; Janetti et al., 2008) and the validation of snow deposition and snow transport models (Lehning et al., 2008). A further interesting aspect is the development of surface roughness as a function of the variable snow





cover.

*Acknowledgements.* We thank all people who helped during the extensive field work and in data processing. Part of the work has been funded by the Swiss National Science Foundation and the European Community. This work would not have been possible without all colleagues from SLF who contributed to this work in various ways.

## References

Anderton, S. P., White, S. M., and Alvera, B.: Evaluation of spatial variability in snow water equivalent for a high mountain catchment, Hydrol. Process., 18, 435–453, 2004.

Armstrong, R. L. and Brown, R.: Introduction, in: Snow and climate, edited by: Armstrong, R. L. and Brun, E., Cambridge University Press, Cambridge, 1–11, 2008.

Balk, B. and Elder, K.: Combining binary decision tree and geostatistical methods to estimate snow distribution in a mountain watershed, Water Resour. Res., 36, 13–26, 2000.

Bauer, A. and Paar, G.: Monitoring von Schneehöhen mittels terrestrischem Laserscanner zur Risikoanalyse von Lawinen, 14th International Course on Engineering Surveying, Zürich, 15–19 March 2004.

Beniston, M.: Environmental change in mountains and uplands, London UK and Oxford University Press, New York, 2000.

Blöschl, G.: Scaling issues in snow hydrology, Hydrol. Process., 13, 2149–2175, 1999.

Bocchiola, D., Bianchi Janetti, E., Gorni, E., Marty, C., and Sovilla, B.: Regional evaluation of three day snow depth for avalanche hazard mapping in Switzerland, Nat. Hazards Earth Syst. Sci., 8, 685–705, 2008, http://www.nat-hazards-earth-syst-sci.net/8/685/2008/.

Chang, K. T. and Li, Z.: Modelling snow accumulation with a geographic information system, Int. J. Geogr. Inf. Sci., 14, 693–707, 2000.

Dadic, R., Mott, R., Lehning, M., and Burlando, P.: Wind influence on snow distribution and accumulation over glaciers, J. Geophys. Res., doi:10.1029/2009JF001261, in press, 2010.

Deems, J. S., Fassnacht, S. R., and Elder, K. J.: Fractal distribution of snow depth from lidar data, J. Hydromet., 7, 285–297, 2006.

Deems, J. S. and Painter, T. H.: Lidar measurement of snow depth: Accuracy and error sources,





in: Proceedings of the International Snow Science Workshop ISSW, Telluride, CO, USA, 1–6 October 2006, 384–391, 2006.
Doorschot, J., Raderschall, N., and Lehning, M.: Measurements and one-dimensional model calculations of snow transport over a mountain ridge, Ann. Glaciol., 32, 53–158, 2001.
Elder, K., Rosenthal, W., and Davis, R. E.: Estimating the spatial distribution of snow water equivalence in a montane watershed, Hydrol. Process., 12, 1793–1808, 1998.
Erickson, T. A., Williams, M. W., and Winstral, A.: Persistence of topographic controls on the spatial distribution of snow in rugged mountain terrain, Colorado, United States, Water Resour. Res., 41, W04014, doi:10.1029/2003WR002973, 2005.
Essery, R. and Pomeroy, J.: Implications of spatial distributions of snow mass and melt rate for snow-cover depletion: theoretical considerations, Ann. Glaciol., 38, 261–265, 2004.
Fazzini, M., Fratianni, S., Biancotti, A., and Billi, P.: Skiability conditions in several skiing complexes on Piedmontese and Dolomitic Alps, Meteorol. Z., 13, 253–258, 2004.
Haefner, H., Seidel, K., and Ehrler, H.: Applications of snow cover mapping in high mountain regions, Phys. Chem. Earth, 22, 275–278, 1997.
Helbig, N., Löwe, H., and Lehning, M.: Radiosity approach for the shortwave surface radiation balance in complex terrain, J. Atmos. Sci., 66, 2900–2912, 2009.
Hopkinson, C., Sitar, M., Chasmer, L., Gynan, C., Agro, D., Enter, R., Foster, J., Heels, N., Hoffnan, C., Nillson, J., and St.Pierre, R.: Mapping the spatial distribution of snowpack depth beneath a variable forest canopy using airborne laser altimetry, Proceedings of the 58th Eastern Snow Conference, 17–19 May 2001, Ottawa, Ontario, Canada, 2001.
Janetti, E. B., Gorni, E., Sovilla, B., and Bocchiola, D.: Regional snow-depth estimates for avalanche calculations using a two-dimensional model with snow entrainment, Ann. Glaciol., 49, 63–70, 2008.
Jonas, T., Marty, C., and Magnusson, J.: Estimating the snow water equivalent from snow depth measurements in the Swiss Alps, J. Hydrol., 378, 161–167, 2009.
Jones, H. G., Pomeroy, J. W., Walker, D. A., and Hoham, R. W.: Snow ecology: An interdisciplinary examination of snow-covered ecosystems, Cambridge University Press, Cambridge, UK, 378 pp., 2001.
Jörg, P., Fromm, R., and Sailer, R. S. A.: Measuring snow depth with a terrestrial laser ranging system, Proceedings International Snow Science Workshop ISSW 2006, Telluride, CO, USA, 1–6 October 2006, 452–460, 2006.
Keller, F., Kinast, F., and Beniston, M.: Evidence of the response of vegetation to environmental





change at high elevation sites in the Swiss Alps, Regional Env. Change, 1, 70–77, 2000.
Lehning, M., Völksch, I., Gustafsson, D., Nguyen, T. A., Stähli, M., and Zappa, M.: Alpine3d: A detailed model of mountain surface processes and its application to snow hydrology, Hydrol. Process., 20, 2111–2128, 2006.
Lehning, M., Löwe, H., Ryser, M., and Radschall, N.: Inhomogeneous precipitation distribution and snow transport in steep terrain, Water Resour. Res., 44, W07404, doi:10.1029/2007WR006545, 2008.
Liston, E. G. and Sturm, M.: Winter precipitation patterns in arctic Alaska determined from a blowing-snow model and snow-depth observations, J. Hydrometeorol., 3(4), 646–659, 2002.
López-Moreno, J. I. and Nogués-Bravo, D.: Interpolating local snow depth data: An evaluation of methods, Hydrol. Process., 20, 2217–2232, 2006.
Luce, C. H., Tarboton, D. G., and Cooley, K. R.: Sub-grid parameterization of snow distribution for an energy and mass balance snow cover model, Hydrol. Process., 13, 1921–1933, 1999.
Male, D. H. and Gray, D. M.: Snowcover ablation and runoff, in: Handbook of snow, edited by: Gray, D. M. and Male, D. H., Pergamon Press, Toronto, CA, 360–436, 1981.
Marchand, W. D. and Killingtveit, A.: Statistical properties of spatial snowcover in mountainous catchments in Norway, Nord. Hydrol., 35, 101–117, 2004.
Marty, C.: Regime shift of snow days in Switzerland, Geophys. Res. Lett., 35, L12501, doi:10.1029/2008GL033998, 2008.
Merz, R., Parajka, J., and Blöschl, G.: Scale effects in conceptual hydrological modeling, Water Resour. Res., 45, W09405, doi:10.1029/2009WR007872, 2009.
Mott, R., Faure, F., Lehning, M., Löwe, H., Hynek, B., Michlmayr, G., Prokop, A., and Schöner, W.: Simulation of seasonal snow-cover distribution for glacierized sites on Sonnblick, Austria, with Alpine 3D model, Ann. Glaciol., 49, 155–160, 2008.
Mott, R. and Lehning, M.: Meteorological modelling of very high resolution wind fields and snow deposition for mountains, J. Hydromet., in review, 2010.
Pomeroy, J. W. and Gray, D. M.: Snowcover accumulation, relocation and management, Saskatoon, 1995.
Pomeroy, J. W., Toth, B., Granger, R. J., Hedstrom, N. R., and Essery, R. L. H.: Variation in surface energetics during snowmelt in a subarctic mountain catchment, J. Hydromet., 4, 702–719, 2003.
Prokop, A.: Assessing the applicability of terrestrial laser scanning for spatial snow depth measurements, Cold Reg. Sci. Technol., 54, 155–163, 2008.





Prokop, A., Schirmer, M., Rub, M., Lehning, M., and Stocker, M.: A comparison of measurement methods: Terrestrial laser scanning, tachymetry and snow probing, for the determination of spatial snow depth distribution on slopes, Ann. Glaciol., 49, 210–216, 2008.

Raderschall, N., Lehning, M., and Schär, M.: Fine-scale modeling of the boundary layer with wind field over steep topography, Water Resour. Res., 44, W09425, doi:10.1029/2007WR006545, 2008.

Riegl Laser Measurement Systems, G.: Long-range laser profile measuring system LPM-321: Technical documentation & user's instructions, 2008.

Rovansek, R. J., Kane, D. L., and Hinzman, L. D.: Improving estimates of snowpack water equivalent using double sampling, Proceedings of the 61st Western Snow Conference, 8–10 June 1993, Queebeck City, Canada, 1993.

Schaffhauser, A., Fromm, R., Jörg, P., Luzi, G., Noferini, L., and Sailer, R.: Remote sensing based retrieval of snow cover properties, Cold Reg. Sci. Technol., 54, 164–175, 2008.

Skaloud, J., Vallet, J., Keller, K., Veyssière, G., and Kölbl, O.: An eye for landscapes – rapid aerial mapping with handheld sensors, GPS World, 17, 26–32, 2006.

Trujillo, E., Ramirez, J. A., and Elder, K. J.: Topographic, meteorologic, and canopy controls on the scaling characteristics of the spatial distribution of snow depth fields, Water Resour. Res., 43, W07409, doi:10.1029/2006WR005317, 2007.

Vallet, J. and Skaloud, J.: Helimap: Digital imagery/lidar handheld airborne mapping system for natural hazard monitoring, 6 setmana Geomatica, Barcelona, 1–10 February 2005.

Xue, M., Droegemeier, K. K., and Wong, V.: The advanced regional prediction system (ARPS) - a multi-scale nonhydrostatic atmospheric simulation model. Part I: Model dynamics and verification, Meteorol. Atmos. Phys., 75, 161–193, 2000.





**Table 1.** Depth-averaged snow density values $\rho(t)\frac{\text{kg}}{\text{m}^3}$ [kg/m$^2$] for each time step.

| | 26 Apr | 13 May | 2 Jun | 10 Jun |
|---|---|---|---|---|
| $\rho(t)$ | 345.2 | 388.6 | 477.4 | 500.7 |





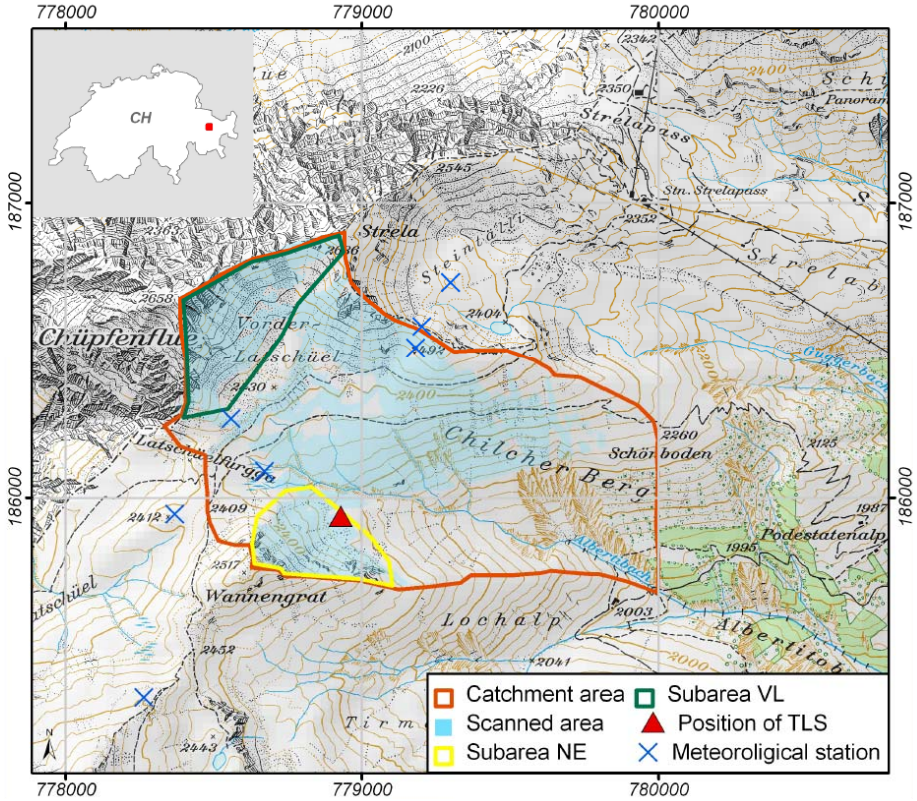


**Fig. 1.** Location of the Albertibach catchment (marked with the red line), the sub-areas NE (yellow line) and VL (green line), the area scanned in the TLS surveys (blue) and the position of the TLS (red triangle) and of the meteorological stations in the area (blue crosses) (base map: Pixelkarte PK25 © 2009 swisstopo (dv033492)).

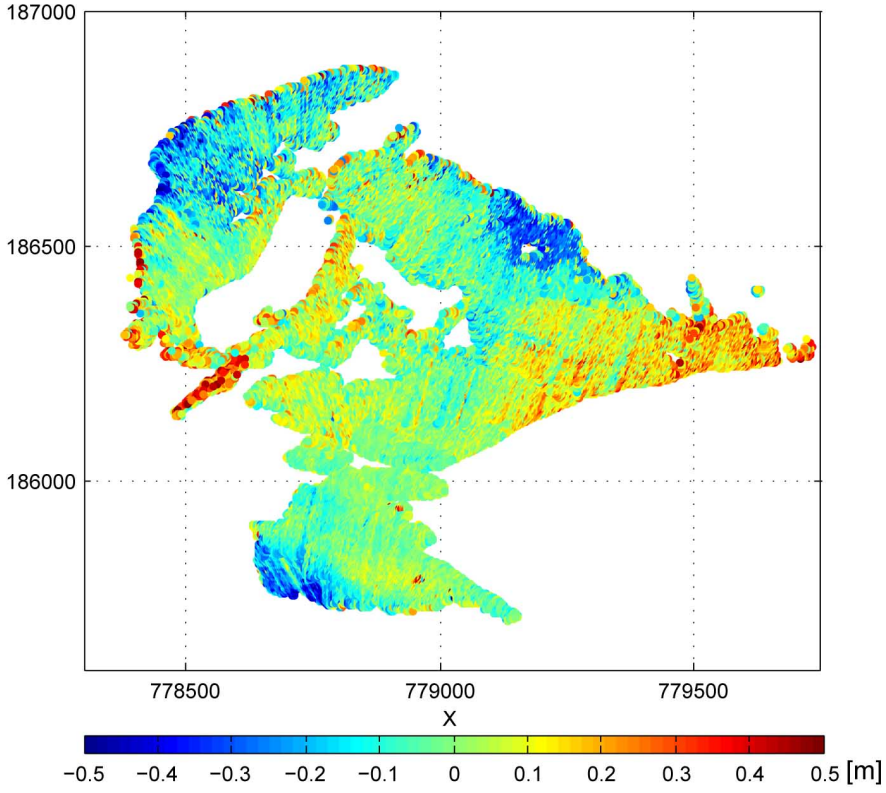


**Fig. 2.** Spatial distribution of the deviation in z-direction [m] between ALS and TLS survey for 26 April 2008.

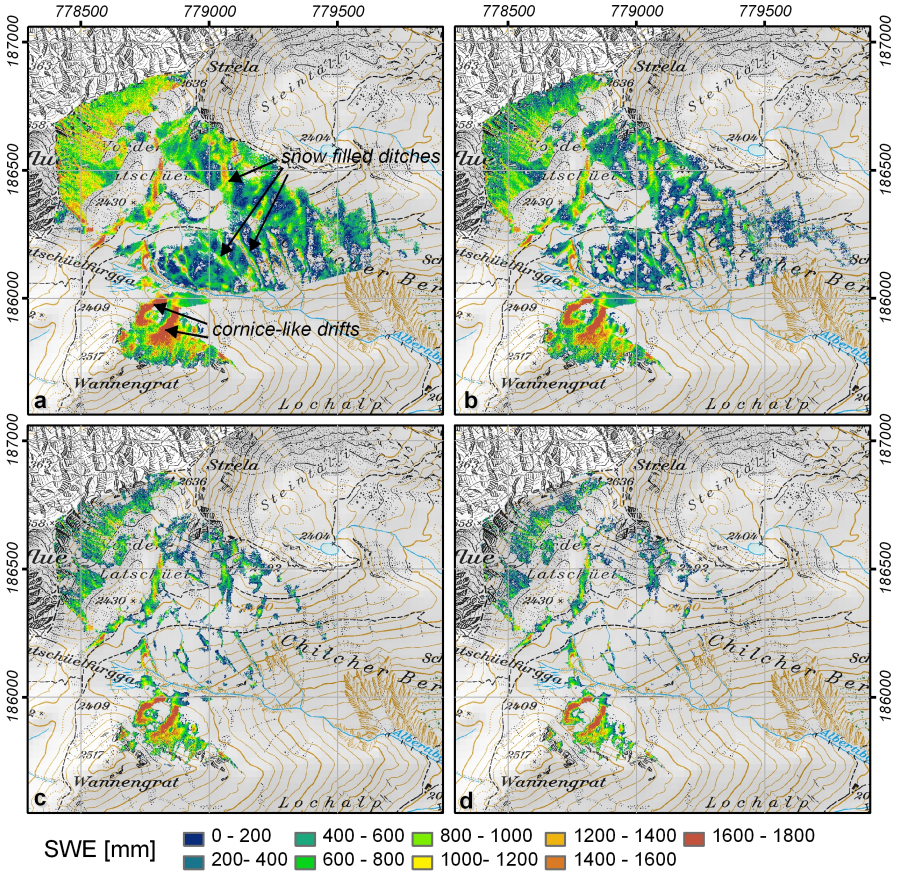


**Fig. 3.** SWE maps for 26 April **(a)**, 13 May **(c)**, 2 June **(c)** and 10 June **(d)**. The black arrows mark examples for snow filled ditches and cornice-like drifts (base map: Pixelkarte PK25 © 2009 swisstopo (dv033492)).

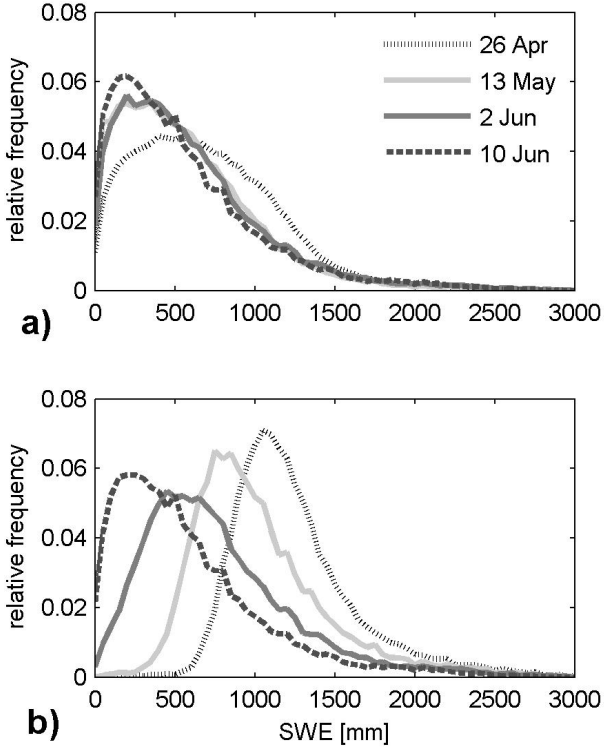


**Fig. 4.** Histograms of SWE for the snow covered area at the time of each scan **(a)** and for those fractions only which had still snow at 10 June **(b)**. Interval size: 63.

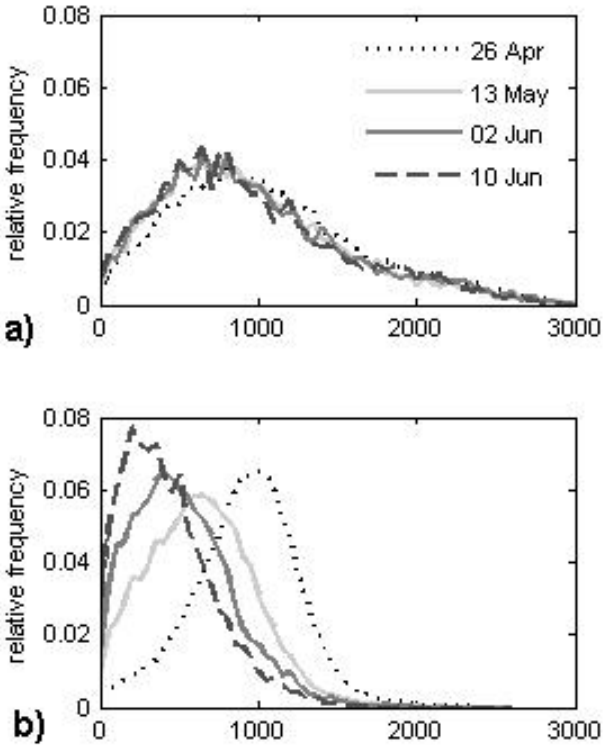


**Fig. 5.** Histograms of SWE for the sub-areas NE **(a)** and VL **(b)**. Interval size for (a): 63, interval size for (b): 53.

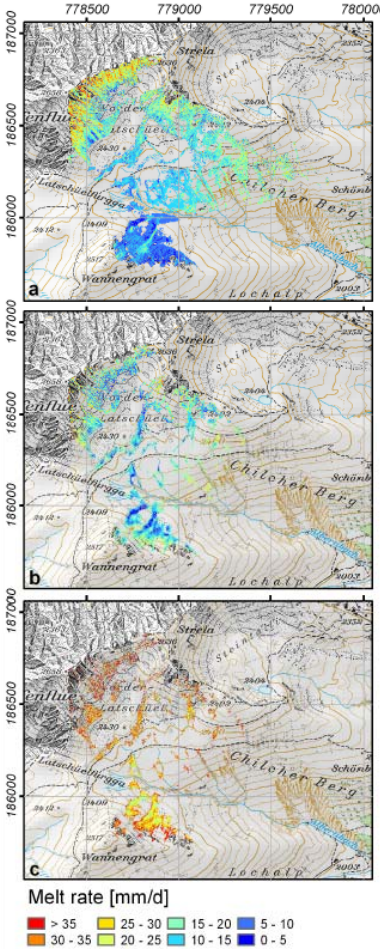


**Fig. 6.** Daily melt rates averaged for the time periods 26 April–13 May **(a)**, 13 May–2 June **(b)** and 2 June–10 June **(c)** (base map: Pixelkarte PK25 © 2009 swisstopo (dv033492)).

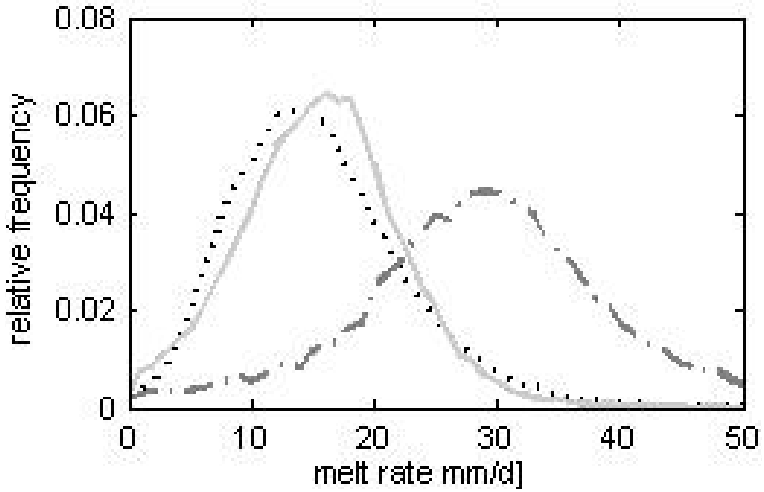


**Fig. 7.** Histograms of daily melt rate for the whole catchment area. Interval size: 124.

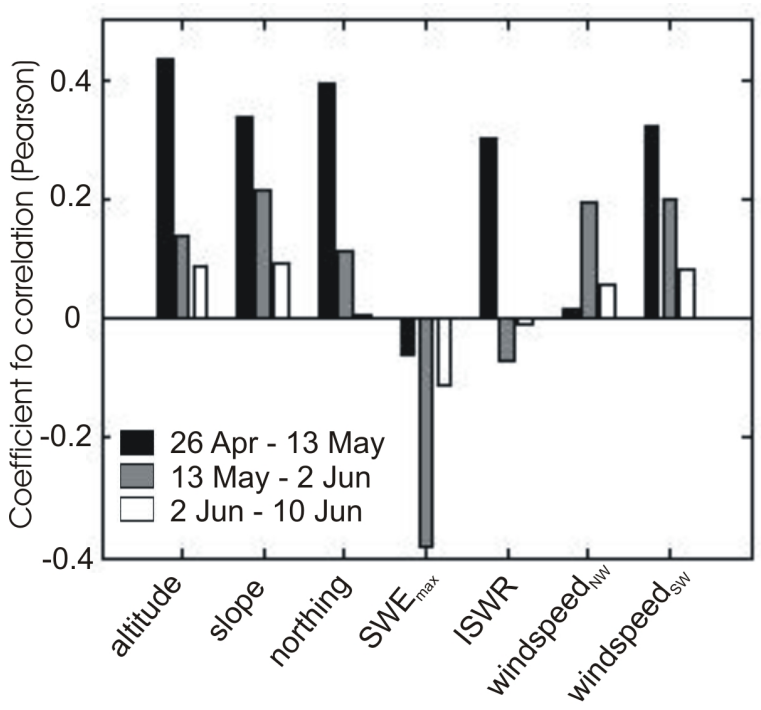


**Fig. 8.** Coefficient of correlation (Pearson) for daily melt rates for each time period against altitude, slope, northing, SWE at the end of the accumulation season ($SWE_{max}$), incoming shortwave radiation for each period (ISWR) and windspeed for prevailing wind direction north-west ($windspeed_{NW}$) and south-west ($windspeed_{SW}$).

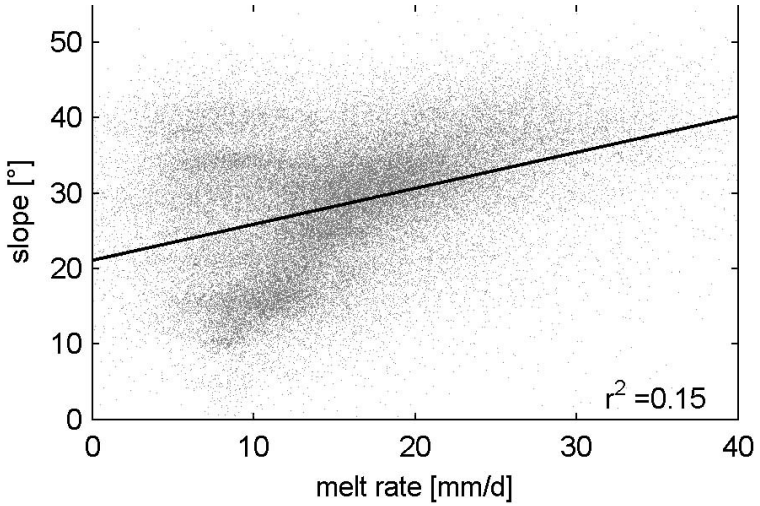


**Fig. 9.** Scatterplot of SWE melt rates (26 April–13 May) and slope angle. The solid line draws the linear fit function derived from the univariate regression analysis.